Dalton Transactions

Accepted Manuscript

ROYAL SOCIETY OF CHEMISTRY

www.rsc.org/dalton

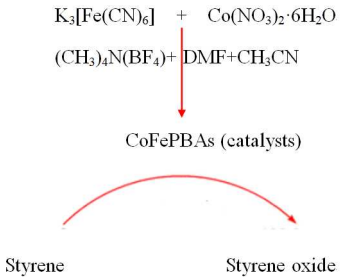

Synthesis and characterization of CoFePBAs in ionic liquid solution and their catalytic properties of styrene epoxidation are presented.

Journal Name

ARTICLE

Simple synthesis of Prussian blue analogues in room temperature ionic liquid solution and their catalytic application in epoxidation of styrene

Received 00th January 20xx,
Accepted 00th January 20xx

DOI: 10.1039/x0xx00000x

www.rsc.org/

Qianqian Wang[a], Ning Wang[a], Sifa He[a], Jihua Zhao[a,]*, Jian Fang[a], Weiguo Shen[a,b]

In this article, a new application of the room temperature ionic liquid, tetramethylammonium tetrafluoroborate, is described. This ionic liquid is used as a stabilizing agent and the reaction medium for the synthesis of CoFe Prussian blue analogues nanoparticles using *N*, *N*-dimethyl formamide as a complexing agent. The so-synthesized Prussian blue analogues were characterized by various techniques and were used to catalyze the reaction of epoxidation of styrene. The catalytic activity of Prussian blue analogues prepared in ionic liquid was superior to that of Prussian blue analogues prepared in aqueous solution.

1. Introduction

Prussian blue analogues (PBAs), with a general formula of $A_hM_k[M'(CN)_6]_l \cdot mH_2O$ (h, k, l, m=stoichiometric numbers; A=alkali metal cation; M, M′=transition metal ions), are formed by replacing one or more of the iron centers of Prussian blue by other transition metals. Most of the Prussian blue analogues have been first studied due to their properties as molecule-based magnets.[1-3] Later, PBAs formed a unique class of materials that have received a great attention because of their various interesting properties, such as photomagnetism,[4, 5] magnetic pole inversion,[6, 7] and possible technological applications of hydrogen storage,[8] batteries materials,[9, 10] and electro- and photocatalysis.[11] At present, the synthesis methods of PBAs are diverse, and significantly influence their structure and properties. Main methods are as follows: (1) precipitation, (2) electrochemical deposition, (3) hydrothermal method, (4) microemulsion method, (5) microwave method, (6) ultrasonic method, and so on.

Ionic liquids (ILs) have attracted increasing attention due to their unique intrinsic properties, such as a negligible vapor pressure, a large liquid temperature range, an ability of dissolving a variety of chemicals, a high thermal stability, a large electrochemical window, and a potential as "designer solvents" and "green" replacements of volatile organic solvents.[12-15] Taking into account these properties, ILs are widely used in the chemical and mechanical industries, catalysis, electrochemistry and separation technologies.[16-20] In recent years, ionic liquids have been discovered to be excellent media in the formation and stabilisation of metallic and metal oxide nanosized objects.[21] For instance, compared with other preparation methods, higher catalytic activities were achieved when Pt–Ru/C catalysts were prepared in ionic liquids, and when carbon nanotube-supported noble metal nanoparticles were synthesized with an ionic-liquid-assisted method.[22, 23]

Herein, we report a simple and efficient synthetic method of CoFePBA nanoparticles (NPs) using the ionic liquid, tetramethylammonium tetrafluoroborate, which acts as a stabilizing agent and the reaction medium. We also studied their catalytic application for the epoxidation of styrene. The structural and morphological analysis of PBA NPs have been characterized by Fourier transform infrared spectroscopy (FT-IR), X-ray diffraction (XRD), Energy Dispersive Spectrometer (EDS), Elemental analysis (EA), N_2-adsorption/desorption, Transmission electron microscopy (TEM), Scanning electron microscopy (SEM) and Thermal gravimetry (TG).

[a.] *Address here.*
[b.] *Address here.*
[c.] *Address here.*

† Footnotes relating to the title and/or authors should appear here. Electronic Supplementary Information (ESI) available: [details of any supplementary information available should be included here]. See DOI: 10.1039/x0xx00000x

2. Experimental

2.1. Materials

Cobalt nitrate hexahydrate (Sinopharm Chemical Reagent Co. Ltd, China, ≥99.0%), Potassium ferrocyanide (Tianjin Guangfu Fine Chemical Research Institute, China, ≥99.0%), *N*, *N*-dimethyl formamide (DMF, ≥99.5%), ethanol (≥99.7%) and acetonitrile (≥99.9%) were all analytical grade and used without further purification. Tert-butyl hydroperoxide (TBHP, ≥70.0%) was chemical grade and used without further purification. Styrene (≥99.0%) was chemical grade and distilled prior to use. Tetramethylammonium tetrafluoroborate with a purity of 99.0% was used as received from Shanghai Chengjie Co. Ltd. Double distilled water was used throughout this study.

2.2. Synthesis of CoFePBA-1 in aqueous solution

25 mL of a 10 mmol L^{-1} solution of $K_3[Fe(CN)_6]$ was slowly added to 25 mL of a 10 mmol L^{-1} solution of $Co(NO_3)_2 \cdot 6H_2O$ at 25 ℃ in water under magnetic stirring. The mixture was stirred for 2 h. Then, the precipitates were collected by centrifugation and washed with distilled water and ethanol several times. After drying at room temperature, the resulting powder was named as CoFePBA-1.

2.3. Synthesis of CoFePBA-2 in ionic liquid

In a typical synthesis, a solution A of $Co(NO_3)_2 \cdot 6H_2O$ (0.22 mmol) and 0.1200 g of $(CH_3)_4N(BF_4)$ (tetramethylammonium tetrafluoroborate) in 10 mL of acetonitrile was added to a solution B of $K_3[Fe(CN)_6]$ (0.15 mmol) and 0.1800 g of $(CH_3)_4N(BF_4)$ (tetramethylammonium tetrafluoroborate) in 15 mL of acetonitrile, under stirring. After stirring for 2 h at room temperature, the mixture was centrifuged and the supernatant solution was decanted. The remaining solid was washed thoroughly with distilled water and acetonitrile several times and dried in air at room temperature to give the product CoFePBA-2.

2.4. Synthesis of CoFePBA-3 in ionic liquid with the complexing agent DMF

Solution A was added to solution B (solution A and solution B are the same as those of 2.3) under stirring. Then, 10 mL of DMF was added into the above solution. After addition, the mixture was stirred continuously for 2 h and the microcrystalline powder was then isolated by centrifugation. The precipitates were rinsed thoroughly several times with distilled water and acetonitrile, and dried under ambient temperature. The final product was denoted as CoFePBA-3.

2.5. Catalytic epoxidation reaction

3 mg of PBA catalysts, 2 mL of acetonitrile, 0.5 mmol of styrene, 0.75 mmol of TBHP as oxidant were added to a 10 mL round bottom flask, equipped with a cooling-water condenser. Then the mixture was stirred at 72 ℃ (oil bath temperature). After 6 h of reaction, the catalyst was separated by centrifuging the reaction mixture, and the liquid organic products were identified and quantified by gas chromatography.

2.6. Characterization

Powder X-ray diffraction (XRD) diffractograms were collected on a Rigaku D/max-2400 X-ray diffractometer with graphite monochromatic Cu-Ka radiation (λ=0.15406 nm). Fourier Transform Infrared Spectroscopy (FT-IR) of dried particles pressed into KBr pellets were obtained on a NICOLET NEXUS-670-FT-IR spectrometer. Transmission electron microscopy (TEM) images were obtained from a Philips Tecnai G2 F20 microscope. Scanning electron microscopy (SEM) images were obtained from a JSM-6701F. Energy Dispersive Spectrometer (EDS) experiments were performed with a JEOL JSM-5600LV. Thermal gravimetry (TG) experiments were performed with a LINSEIS STA PT1600 thermal analyzer. Elemental analysis (EA) measurements were performed on a Vario EL elemental analyzer. N_2-adsorption/desorption isotherms were measured at 77 K with a Quadrachrome Adsorption Instrument. The specific surface area was calculated by the Brunauer–Emmett–Teller (BET) method. Pore size distribution was calculated by the Barrett–Joyner–Halenda (BJH) method.

3. Results and Discussion

3.1. FT-IR spectroscopy characterization

The FT-IR spectra of the CoFePBAs synthesized under different conditions are shown in Fig. 1. In Fig. 1(a), the absorption peaks at 2158.2 cm^{-1} and 2113.5 cm^{-1} of CoFePBA-1, synthesized in aqueous solution, can be assigned to the stretching of the CN group in the Fe^{3+}-CN-Co^{2+} and Fe^{2+}-CN-Co^{3+} environments, respectively.[5, 24] The OH stretching vibration and bending vibration of the water molecules could be observed at the peaks around 3411.1 cm^{-1} and 1608.0 cm^{-1}, respectively. While in the far-IR region, Fe-CN flexural vibration absorption and Co-CN flexural vibration absorption appears at 592.4 cm^{-1}, 431.1 cm^{-1}, respectively. Fig. 1(b) and (c) are the infrared spectrogram of the particles synthesized in ionic liquid without and with the complexing agent DMF. Compared with CoFePBA-1, the characteristic absorption peak for Fe^{3+}-CN-Co^{2+} at 2158.0 cm^{-1} disappears in CoFePBA-2 and CoFePBA-3. The change may be coming from the interaction of ionic liquid and CoFePBAs. The peaks at 2118.7 cm^{-1} and 2122.8 cm^{-1}, corresponding to CoFePBA-2 and CoFePBA-3 respectively, are the characteristic absorption peaks of Fe^{2+}-CN-Co^{3+}. The adsorption band around 1364.1 cm^{-1} refers to the C-N vibration of the quaternary ammonium salt, tetramethylammonium tetrafluoroborate, in CoFePBA-2 and CoFePBA-3 samples. The presence of DMF for CoFePBA-3 is manifested by the low-intensity adsorption band at 1304.6

cm^{-1} that can be connected with the vibration absorption peak of the C-N bound in the amide.

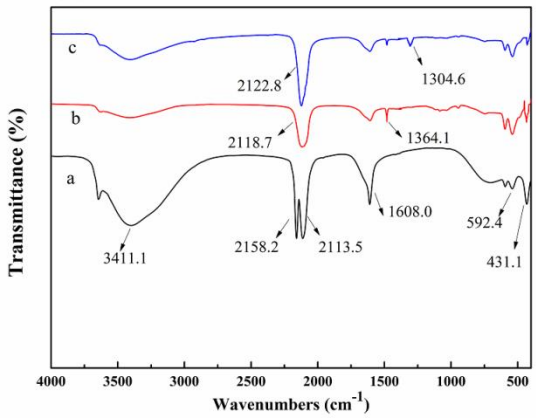

Fig. 1 FT-IR spectra of: (a) CoFePBA-1; (b) CoFePBA-2; (c) CoFePBA-3.

3.2. Morphology analysis

Fig. 2 shows TEM images of the three CoFePBA samples and the SEM image of CoFePBA-3. It could be found that the sizes of CoFePBA-1, CoFePBA-2 and CoFePBA-3 decrease orderly. The CoFePBA-1 NP width was about 200 nm, while the CoFePBA-2 NP width was about 40 nm and the CoFePBA-3 NP width was about 20-30 nm. At 25 ℃, the surface tension of tetramethylammonium tetrafluoroborate is about 40 $mN \cdot m^{-1}$ and the one of water is about 72 $mN \cdot m^{-1}$.[25, 26] As the lower surface tension leads to higher nucleation rates,[27] the sizes of CoFePBA-2 and CoFePBA-3 are much smaller than the size of CoFePBA-1. The size of CoFePBA-3 synthesized with DMF (see Fig. 2(C)) is the smallest, which indicates that the complexing agents act as a protecting agent and prevent particles to grow or aggregate.

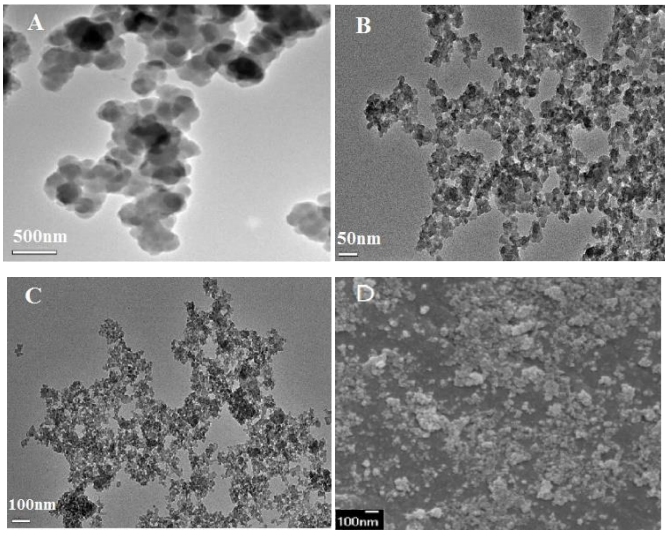

Fig. 2 TEM micrographs of: CoFePBA-1 (A); CoFePBA-2 (B); CoFePBA-3 (C); and SEM micrograph of CoFePBA-3 (D).

3.3. XRD analysis

To explore the crystallinity and phase composition, the CoFePBA samples synthesized under different conditions were analyzed by powder X-ray diffraction (Fig. 3). The XRD pattern of CoFePBA-1 is shown in Fig. 3(a). The sharp intense peaks at 17.5°, 24.8°, 35.4°, 39.8°, correspond to the (200), (220), (400) and (420) scattering reflections, respectively, demonstrating the face-centered cubic (fcc) structure of CoFePBA-1. Meanwhile, the sharpness and the strong intensity of the diffraction peaks confirm the crystallization with high quality. The XRD patterns of CoFePBA-2 and CoFePBA-3 in Fig. 3(b) and (c) show four main diffraction peaks, apparently indicating the fcc structure, but the crystallization quality of CoFePBA-2 and CoFePBA-3 is much poorer than that of CoFePBA-1. It is speculated that the low surface tension of tetramethylammonium tetrafluoroborate influences the crystallinity of the materials.[27]

According to the Scherrer's formula, the crystallite sizes of CoFePBA-2 and CoFePBA-3 are about 32 nm and 20 nm, respectively, which are consistent with the results from TEM measurement. By contrast, the size of CoFePBA-1 could not be obtained from the Scherrer's formula, as the material possesses diameter larger than 100 nm.

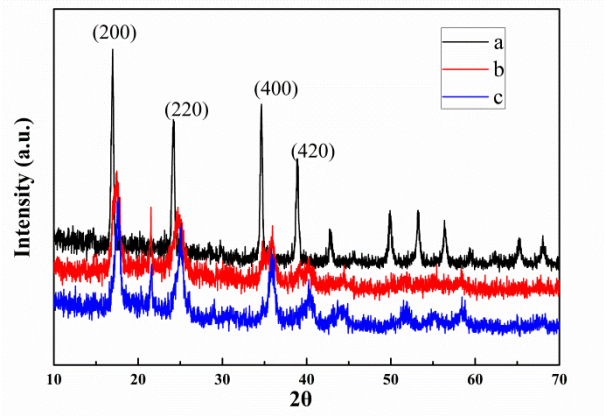

Fig. 3 XRD patterns of: (a) CoFePBA-1; (b) CoFePBA-2; (c) CoFePBA-3.

3.4. N_2-adsorption/desorption analysis

Fig. 4 and Table 1 show the nitrogen adsorption–desorption isotherms, the BJH pore size distribution and the specific surface area of the CoFePBAs synthesized under different conditions, respectively. From Fig. 4(A), the adsorption isotherms of the three CoFePBAs all belong to type IV with a H3 type hysteresis loop, with pore sizes smaller than 50 nm, indicating the existence of some mesopores in the CoFePBAs' structure. From Table 1, it can be seen that the BET surface

areas of the CoFePBA-1, CoFePBA-2 and CoFePBA-3 powders are 18.1, 97.9 and 124.5 $m^2 g^{-1}$, respectively. Clearly, the BET surface area of CoFePBA-3, which was synthesized in ionic liquid with the complexing agent DMF, is the largest, whereas that of CoFePBA-1, synthesized in aqueous solution, is the smallest. It is well known that the smaller particle has bigger specific surface area. Hence the observation is in agreement with the fact that the particle size of CoFePBA-1 is the largest and that of CoFePBA-3 is the smallest.

the loss of the surface residual ionic liquid structure in CoFePBA.[28-31] Stage III (329.7-686.8 ℃) (34.4%) is similar to the Stage II and Stage III of CoFePBA-1. The thermogravimetric curve of CoFePBA-3 is similar with CoFePBA-2 except the Stage I (50-158.9 ℃) (11.6%), which is the removal of coordinating water and complexing agent DMF molecules. Obviously, the final decomposition temperature of Stage III in CoFePBA-2 and CoFePBA-3 is higher than CoFePBA-1. The main reason is that IL could provide a suitable medium for the stabilization of various nanoparticles.[21, 32]

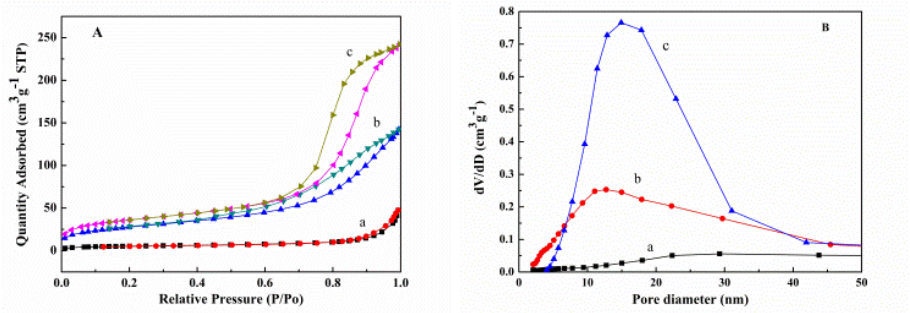

Fig. 4 N_2-sorption isotherms (A) and pore size distributions (B) of CoFePBAs: (a) CoFePBA-1; (b) CoFePBA-2; (c) CoFePBA-3.

Table 1 N_2-adsorption/desorption results of the three CoFePBAs.

Run	BET Surface Area ($m^2 g^{-1}$)	Pore Size (nm)
CoFePBA-1	18.1	23.8
CoFePBA-2	97.9	9.1
CoFePBA-3	124.5	10.3

3.5. Thermal gravimetry (TG) characterization

As shown in Fig. 5, thermogravimetric curves of the CoFePBAs were conducted in the temperature range from 0 to 800 ℃. In CoFePBA-1, there are three main stages of weight loss: stage I (50-170.2 ℃), stage II (244.4-427.8 ℃), and stage III (427.8-544.3 ℃). Stage I is the complete removal of coordinating water molecules (weight loss of 22.4%); Stage II is caused by the decomposition of the cyanide group, followed by the transformation of the double metal cyanide complexes into metal nitrates (weight loss of 15.2%); Stage III is the complete decomposition of the materials into metal oxide (weight loss of 22.1%). Compared with CoFePBA-1, CoFePBA-2 and CoFePBA-3 also have three stages of weightlessness. The differences are the temperature of weightlessness and the component of weightlessness. In CoFePBA-2, stage I (50-152 ℃) (9.9%) is the removal of a little water. Stage II (152-329.7 ℃) (4.3%) is

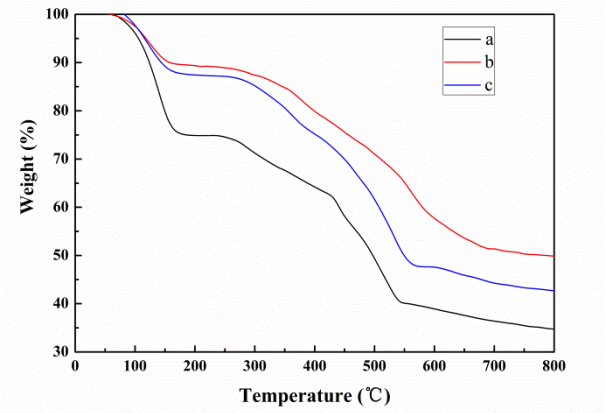

Fig. 5 TG curves of: (a) CoFePBA-1; (b) CoFePBA-2; (c) CoFePBA-3.

3.6. Energy Dispersive Spectrometer (EDS) and Elemental analysis (EA) characterizations

Results of EDS and EA are listed in Table 2 and Table 3, respectively. From the EDS, TG and EA characterizations, the molecular formulas of the synthesized CoFePBAs are as follows:

CoFePBA-1:

$K_{0.036}Co_{1.55}[Fe(CN)_6]\cdot 5.94H_2O$

CoFePBA-2:

$K_{0.53}Co_{1.40}[Fe(CN)_6]\cdot 3.78H_2O\cdot 0.18C_4H_{12}BF_4N$

CoFePBA-3:

$K_{0.96}Co_{1.08}[Fe(CN)_6]\cdot 3.49H_2O\cdot 0.16DMF\cdot 0.07C_4H_{12}BF_4N$

From the above molecular formulas, it is found that the number of water molecular of CoFePBA-1, which was synthesized in aqueous solution, is much larger than those of CoFePBA-2 and CoFePBA-3, which were synthesized in ionic liquid. And ionic liquid both remain in CoFePBA-2 and CoFePBA-3; nevertheless, the residual amount of $C_4H_{12}BF_4N$ in CoFePBA-3 is lower than that of CoFePBA-2, for the existing of DMF in CoFePBA-3.

Table 2 EDS results of the three CoFePBAs.

Run	K (wt %)	Fe (wt %)	Co (wt %)	C (wt %)	N (wt %)	O (wt %)	F (wt %)
CoFePBA-1	0.59	16.17	25.12	29.96	24.61	3.55	-
CoFePBA-2	7.45	13.93	19.53	28.45	21.11	4.83	4.06
CoFePBA-3	13.28	13.84	14.88	29.51	20.82	4.73	2.93

Table 3 EA results of the three CoFePBAs.

Run	C (wt %)	H (wt %)	N (wt %)
CoFePBA-1	17.21	2.85	19.98
CoFePBA-2	19.31	2.01	22.09
CoFePBA-3	19.31	2.03	21.5

3.7. Catalytic application

The catalytic properties of the CoFePBAs for the epoxidation of styrene with 70% TBHP are demonstrated in Table 4.

Table 4 Effect of the three CoFePBAs on the epoxidation of styrene

Run	Styrene conversion (%)	Selectivity (%)	
		Styrene oxide	Benzaldehyde
CoFePBA-1	64	26	74
CoFePBA-2	84	27	73
CoFePBA-3	92	40	60

Reaction conditions: catalyst (3 mg), styrene (0.5 mmol), TBHP (0.75 mmol), tempt.=345 K, time=6 h.

CoFePBA-3 achieved the highest conversion of styrene (92%) and the best selectivity in epoxide (40%). The conversion rate of CoFePBA-2 is higher than the one of CoFePBA-1, while the selectivity with CoFePBA-1 and CoFePBA-2 is analogous. It could be concluded that the catalytic activity of the three catalysts has the following sequence: CoFePBA-3 > CoFePBA-2 > CoFePBA-1, that is, the catalytic activity of CoFePBA-3 synthesized in ionic liquid with the complexing agent (DMF) is the best, and CoFePBA-1 synthesized in aqueous solution is the lowest. From N_2-adsorption/desorption, the BET surface areas of the CoFePBAs follow the order: CoFePBA-3 > CoFePBA-2 > CoFePBA-1. On the contrary, the particle size of CoFePBA-3 is the smallest and the one of CoFePBA-1 is the biggest. These results confirm that a larger specific surface area, related to a smaller particle size, is favorable to the catalytic activity, ensuring a better dispersion and a better exposure of the active sites to the reactants. [33-35] Additionally, from the results of XRD, we get the conclusion that the crystallizations of CoFePBA-2 and CoFePBA-3 are much worse than the one of CoFePBA-1, and poor crystallization is usually benefit for the catalytic activity. [36-38] Compared to catalyst with high crystallization, there are more surface defects and active sites in catalyst with poor crystallization. Then it will be more easily for substrate to adsorb and coordinate, so poor crystallization is usually benefited for the catalytic activity. Comprehensive above, the specific surface area, the particle size and the crystallization are the key factors of the catalytic effect.

4. Conclusions

In this work, we have successfully synthesized CoFePBA NPs in a room temperature ionic liquid, and we used these CoFePBA NPs to catalyze styrene epoxidation reaction. The result demonstrates that the catalytic activity of CoFePBA synthesized in ionic liquid with the complexing agent DMF is high, due to a large BET surface area, a small NP size and a poor crystallization. This method reveals a perfect shortcut in the synthesis of PBA networks compared with conventional ways in aqueous solution. Overall, this study extends the application of ionic liquid methods as a convenient way to synthesize catalysts and to improve the corresponding catalytic activity.

Acknowledgements

Financial support was provided by the National Natural Science Foundation of China (Projects 20603014 and 21403098) and the Fundamental Research Funds for the Central Universities (Project lzujbky-2011-116).

References

1. T. Mallah, S. Thiebaut, M. Verdaguer and P. Veillet, *Science*, 1993, **262**, 1554-1557.

2. W. R. Entley and G. S. Girolami, *Science*, 1995, **268**, 397-400.
3. S. Ferlay, T. Mallah, R. Ouahes, P. Veillet and M.Verdaguer, *Nature*, 1995, **378**, 701-703.
4. O. Sato, T. Iyoda, A. Fujishima and K. Hashimoto, *Science*, 1996, **272**, 704-705.
5. N. Shimamoto, S. Ohkoshi, O. Sato and K. Hashimoto, *Inorg. Chem.*, 2002, **41**, 678-684.
6. S. Ohkoshi, Y. Abe, A. Fujishima and K. Hashimoto, *Phy. Rev. Lett.*, 1999, **82,** 1285-1288.
7. S. M. Yusuf, A. Kumar and J. V. Yakhmi, *Appl. Phys. Lett.*, 2009, **95**, 182506-182506-3.
8. S. S. Kaye and J. R. Long, *J. Am. Chem. Soc.*, 2005, **127**, 6506-6507.
9. C. D. Wessells, R. A. Huggins and Y. Cui, *Nat. Commun.*, 2011, **2**, 550.
10. Y. Lu, L. Wang, J. Cheng and J. B. Goodenough, *Chem. Commun.*, 2012, **48**, 6544-6546.
11. K. Itaya, N. Shoji and I. Uchida, *J. Am. Chem. Soc.*, 1984, **106**, 3423-3429.
12. T. Welton, *Chem. Rev.*, 1999, **99**, 2071-2083.
13. M. J. Earle and K. R. Seddon, *Pure. Appl. Chem.*, 2000, **72**, 1391-1398.
14. J. Dupont, R. F. de Souza and P. A. Z. Suarez, *Chem. Rev.*, 2002, **102**, 3667-3692.
15. R. D. Rogers and K. R. Seddon, *Science*, 2003, **302**, 792-793.
16. J. M. Crosthwaite, S. N. V. K. Aki, E. J. Maginn and J. F. Brennecke, *J. Phys. Chem. B*, 2004, **108**, 5113-5119.
17. W. Yang, H. Cang, Y. Tang, J. Wang and Y. Shi, *J. Appl. Electrochem.*, 2008, **38**, 537-542.
18. U. Domanska, A. Pobudkowska and M. Krolikowski, *Fluid Phase Equilib.*, 2007, **259**, 173-179.
19. H. Cao, L. McNamee and H. Alper, *J. Org. Chem.*, 2008, **73**, 3530-3534.
20. U. Domanska and A. Marciniak, *J. Chem. Thermodyn.*, 2008, **40**, 860-866.
21. J. Dupont, G. S. Fonseca, A. P. Umpierre, P. F. Fichtner and S. R. Teixeira, *J. Am. Chem. Soc.*, 2002, **124**, 4228-4229.
22. X. Xue, T. Lu, C. Liu, W. Xu, Y. Su, Y. Lv and W. Xing, *Electrochim. Acta*, 2005, **50**, 3470-3478.
23. H. Chu, Y. Shen, L. Lin, X. Qin, G. Feng, Z. Lin, J. Wang, H. Liu and Y. Li, *Adv. Funct. Mater.*, 2010, **20**, 3747-3752.
24. R. O. Lezn, R. Romagnoli, N. R. de Tacconi and K. Rajeshwar, *J. Phys. Chem. B*, 2002, **106**, 3612-3621.
25. H. H. Li, Y. Imai, M. Yamanaka, Y. Hayami, T. Takiue, H. Matsubara and M. Aratono, *J. Colloid Interface Sci.*, 2011, **359**, 189-193.
26. H. Jiang, Y. Zhao, J. Wang, F. Zhao, R. Liu and Y. Hu, *J. Chem. Thermodyn.*, 2013, **64**, 1-13.
27. G. Gebresilassie Eshetu, M. Armand, B. Scrosati and S. Passerini, *Angew. Chem.*, 2014, **53**, 13342-13359.
28. R. Tao, G. Tamas, L. Xue, S. L. Simon and E. L. Quitevis, *J. Chem. Eng. Data*, 2014, **59**, 2717-2724.
29. Y. Cao and T. Mu, *Ind. Eng. Chem. Res.*, 2014, **53**, 8651-8664.
30. S. M. Sadeghzadeh and F. Daneshfar, *J. Mol. Liq.*, 2014, **199**, 440-444.
31. S. Xun, W. Zhu, D. Zheng, L. Zhang, H. Liu, S. Yin, M. Zhang and H. Li, *Fuel*, 2014, **136**, 358-365.
32. Z. Qin, Y. Fang, Y. Wang, H. Li and J. Liang, *Micropor. Mesopor. Mater.*, 2015, **207**, 78-83.
33. R. J. Wei, X. H. Zhang, Y. Y. Zhang, B. Y. Du, Z. Q. Fan and G. R. Qi, *RSC Adv.*, 2014, **4**, 3188-3194.
34. X. H. Zhang, R. J. Wei, X. K. Sun, J. F. Zhang, B. Y. Du, Z. Q. Fan and G. R. Qi, *Polymer*, 2011, **52**, 5494-5502.
35. J. Sebastian and D. Srinivas, *Appl. Catal. A-Gen.*, 2013, **464-465**, 51-60.
36. W. Zhang, Q. Lin, Y. Cheng, L. Lu, B. Lin, L. Pan and N. Xu, *J. Appl. Polym. Sci.*, 2012, **123**, 977-985.
37. Y. J. Huang, G. R. Qi and L. S. Chen, *Appl. Catal. A-Gen.*, 2003, **240**, 263-271.
38. I. Kim, M. J. Yi, K. J. Lee, D-W. Park, B. U. Kim and C-S. Ha, *Catal. Today*, **2006**, 111, 292-296.